Abstract

The needs for analysis and diagnosis of liquid samples are always great. Tasks can range from determining concentrations of salt and sugar in an industrial process to detecting possibly dangerous pollutants in drinking water. Various methods for these analyses have been developed over the years. Non-invasive methods are very interesting in the perspective that they do not alter the liquid that is analyzed. There is no pollution of the sample. Optical methods often have the advantage to be non-invasive.

Optical methods utilize the fact that the optical properties, such as refractive index and absorption, of a sample may change if a substance is added. The optical methods are often constrained to measure only a few of all the different properties due to cross-talk. Cross-talk is when a measured property is changed because of a change in a different property. The aim of the combinatorial light path spectrometer is to be able to circumvent this issue. This is done by acquiring many measurements values from unique light paths so that the optical properties can be differentiated.

The main purpose of this master thesis was to continue development of a combinatorial light path spectrometer and prove that it was able to measure concentrations of different substances that change the optical properties in a liquid. This was in fact proved to some extent and the results are described in this report.

Contents

Chapter 1

Introduction

1.1 Background

Optical properties of materials have been used in all times to determine physical properties and characteristics of a material at hand. Examples range from looking at the color of hot metal to able to distinguish if it is ready to be forged into a desirable shape to today's measurements of absorption for determination of gas concentrations [1]. The methods for measurements of optical properties have evolved over the years from just looking at the sample with the eyes to the modern high precision spectrometers of our times. The need for new methods is always present, making measurements more efficient, e.g. with higher precision and faster.

Using optical properties to determine a quantity of a sample is of great value as it involves minimum influence on the sample reducing possible errors generated when measuring, e.g. measuring the temperature of a flame [2] with a probe will affect the flame shape thereby altering the actual temperature. Another advantage of measuring optical properties is the adaptability. Being able to choose from a wide wavelength range, from ultraviolet to infrared, enables different properties to be measured that are dependent on the wavelength. A sample may exhibit different properties at different wavelengths, e.g. a gas in a sample may have a specific absorption line where the sample in general does not absorb which will allow for concentration measurements of the gas [3].

Important optical properties that can be measured are refractive index, absorption, scattering and fluorescence. A big issue when measuring the optical properties is the crosstalk that may occur, giving rise to in erroneous results. Cross-talk means that a change in one property may change the measured values of other properties without them actually changing. One

example of cross-talk that can occur when measuring the transmission of a sample is if the sample contains fluorescent substances. The total measured transmission may then be higher than 100% because of the fluorescence. Some cross-talk can be avoided by processing the sample in various ways, e.g. chemically, though this procedure is invasive which often is undesirable.

Measurements of optical properties can be of great value in process and quality control of liquids in industry. Determination of the quality of liquids can easily be made to see if unwanted substances are present assuming the optical properties change due to the new substance. In the brewery/dairy industry the cisterns where the liquids are handled are washed regularly with soap and water. To see how long after the wash the produced liquid is affected, a spectroscopic method could be used. This would allow for instantaneous measurements instead of taking samples to a laboratory and analyze them there in a time consuming process. The measurements can also be done continuously without having to interrupt the production process. A measurement technique that can also suppress possible cross-talk and interference between optical properties is also desirable.

In industry, refractive index measurements are used to determine the salinity or sugar concentration of a solution. There are numerous ways to measure the refractive index [4], [5], [6]. Most of these methods require a sample in a cuvette and are easily hindered if the sample is turbid or contains fluorescent substances.

1.2 Scope

This paper will focus on an instrument for quantifying optical properties. The instrument should be able to do near-instantaneous measurements neglecting any cross-talk in turbid liquids, e.g. milk. The construction of the instrument should be aimed at maximizing the possibility to measure all the relevant optical properties discussed, desirably at a low cost for future industrial applications. Light emitting diodes are used as light sources in the instrument described because of their low cost relative to other light sources and wide range of wavelengths possible. Calibration of the instrument will be done using singular value decomposition (SVD), requiring liquids with known optical properties. Verification of the calibration is to be performed. The temperature relation with respect to the light emitting diodes and the photo detectors will be investigated. A possible field test may be conducted to study if the instrument developed is viable to use as an analysis tool for quality control.

1.3 Outline

The paper is divided into some chapters. The first few chapters will be dedicated to the background theory that is needed to understand the problem that a measurement of different optical properties poses. The first chapter will explain the basics of light and how it can interact with matter and how information about the matter can be gathered from this. Practical techniques used presently for determining the optical properties will be given in the following chapter as well as their limitations.

The mathematical knowledge needed to analyze the measurements is described in the following chapter. An important part in this work is the semi-conductor, e.g. as light source and detector. This is way a chapter is assigned to this important material of the electronics of today.

The following chapter will describe the design of the instrument and how the optical properties are all being able to be measured. Measurements that were conducted in this thesis work are presented and the results are reported and discussed. An overview of how the instrument has faired is given, and lastly, an outlook of possible improvements and modifications that can be done will be suggested.

Chapter 2

Light

In this chapter the basic principles of light will be described, including what properties affect the light and how this can be used to characterize a sample. Light is of a dualistic nature and it can be perceived to have both particle properties and wave properties dependent on how the light is examined. The light can be describe by electromagnetic wave theory according to Maxwell's equations, where one property such as wavelength can describe the energy of the light. The visible region of light lies between 400 nm and 700 nm.

2.1 Energy configuration

When light interacts with matter it is the properties of the atom or molecule that decides what the result will be. From basic atomic physics it is known that an atom consists of a nucleus made up of positively charged particles called protons and neutral particles called neutrons. Around the nucleus electrons are orbiting, giving rise to states called energy levels. The energies of these levels can be calculated using the Schrodinger equation. These levels are also dependent on a variety of factors, e.g. isotope number and external electrical or magnetic fields.

A molecule consists of two or more atoms resulting in a more complex structure. The molecules are created because the total energy of the molecule is lower than if the atoms where separated. The complex structure of molecules gives rise to more possible energy levels. The molecules can in contrast to atoms rotate, if there is at least one axis that they are not symmetric around. This gives rise to rotational energy levels. The atoms in a molecule can also oscillate which gives rise to vibrational energy levels [7]. For liquid and solid materials the spectra have very broad features and not as in gases where absorption lines are very narrow.

2.2 Refraction

The refractive index is a measure of how fast light propagates through a medium. In a medium with refractive index n the reduced speed of light in the medium is given by $c_r = c/n$, where c is the speed of light in vacuum. When light passes between two different media with different refractive indices, part of the light will be reflected and part of the light will be transmitted. The different parts can be calculated using the Fresnel equations. A simplified case is when the light falls perpendicular into the surface. Then the reflection is given by Eq. 2.1, where n_1 and n_2 are the refrective indices for the two media. For more general cases the Kramer-Kronig relation can be used to calculate the refractive index assuming the absorption coefficient can be measured. As it is possible to measure the absorption over a wide frequency range the refractive index can be calculated for the same frequencies.

$$R = \left(\frac{n_1 - n_2}{n_1 + n_2}\right)^2 \tag{2.1}$$

If the light passes between two media with different refractive indices the light will be refracted according to Snell's law. This will occur due to the fact that the light will take the fastest way between two points in space and as the velocity of the light varies the light will take differently long paths in the two media.

The refractive index is dependent on the wavelength of light which will give rise to chromatic dispersion, i.e. different wavelengths will have different velocities in the medium. If white light propagates through water, shorter wavelengths will propagate slower than longer wavelengths. Fig. 2.1 shows how the refractive index for water varies depending on the wavelength.

2.3 Absorption and emission

Absorption of a photon can occur when its energy matches the energy gap between two levels in an atom or molecule. The photon will excite an atom by forcing an electron to transition to a higher energy level. For a molecule there can be both an electron transition and/or an increase in atomic internal movement such as vibration and rotation as a result of excitation. When light is transmitted through an absorbing material the light is attenuated according to the Beer-Lambert law; Eq. 2.2 [9].

$$I = I_0 e^{-\alpha L} \tag{2.2}$$

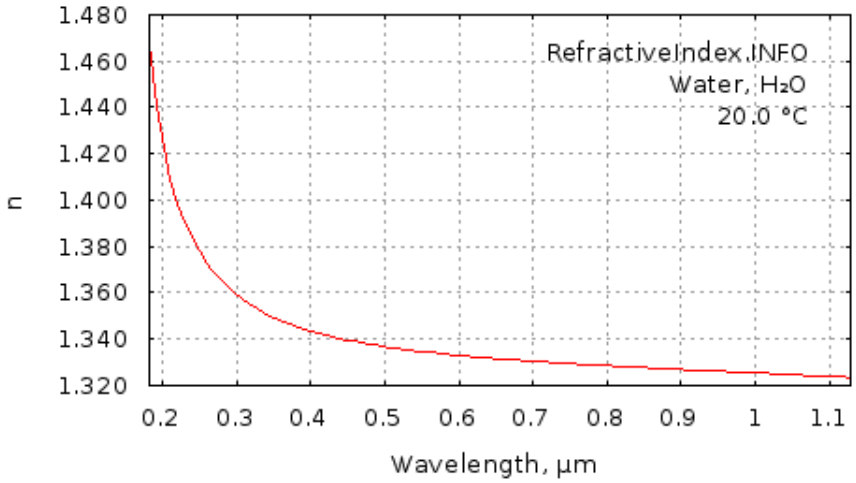

Figure 2.1: Refractive index for 20^o C water depending on the wavelength, from the near-UV to the near-IR region. From [8]

Here I is the detected light, I_0 the incoming light, α the attenuation coefficient and L the length which the light has passed through the medium.

If an incoming photon matches the energy gap between two levels and the electron is situated in the upper of these states the photon can stimulate the electron to fall down and thereby create another photon of the exact same frequency and phase. This is called stimulated emission and is the principle behind lasers. Another form of emission is spontaneous emission, where an excited electron falls, down as the name explains, spontaneously. An excited atom has a limited lifetime that is dependent on the probability of the spontaneous emission.

2.4 Scattering of light

Scattering of light may occur when light interacts with matter. The scattering effect causes light to change propagation direction. There are different types of scattering, elastic and inelastic scattering. For elastic scattering there are negligible energy losses for the light during the scattering event. Examples of elastic scattering are Rayleigh scattering and Mie scattering. For inelastic scattering events the energy of the outgoing photon is changed, either increased or decreased. A media, where the light undergoes multiple scattering is called a turbid medium. For these media the Beer-Lambert law can no longer be used to calculate the absorption due to an unknown

path length, which complicates the determination of the optical properties. There are techniques that circumvent this unknown path-length problem which will be described later.

2.4.1 Rayleigh scattering

Rayleigh scattering can happen when light interacts with particles of smaller size than the wavelength of the interacting light. Typically, the limit to how large the particle size can be is 1/10th of the wavelength. When Rayleigh scattering occurs, the impinging light excites a particle to a virtual level. The particle is instantaneously deexcited emitting a photon of the same frequency as the absorbed one but in a different direction which creates the scattering effect [10].

More theoretically the Rayleigh scattering can be explained by that the light creates a dipole in the particle that is affected by the light. This will occur due to the fact that the positive and negative charges will be separated due to the electric field of the light. Neglecting the movement of the nuclei because of their relatively much larger mass compared to the electrons, the only charge that is moving is simplified to be the electrons. The particle will be an oscillating dipole acting as an antenna for the incoming light. From electromagnetic field theory it is known that the emitted radiation is proportional to the fourth power of the frequency. This means that Rayleigh scattering is heavily dependent on the wavelength. The dependence is λ^{-4}, i.e. shorter wavelengths will scatter more than longer.

2.4.2 Raman scattering

Raman scattering is an inelastic scattering effect. Precisely as in Rayleigh scattering, the system is excited to another virtual energy level. The difference is that when the molecule is deexcited the electron falls back to a different energy level than where it was before the excitation. This gives either an increase or a decrease in the energy of the scattered light. More energetic light after the scattering is said to be anti-Stokes shifted and less energetic light is said to be Stokes shifted.

2.4.3 Mie scattering

Mie scattering arises when the particles that the light is interacting with is of the same size as the wavelength. The probability of Mie scattering to occur is dependent of the particle radius, index of refraction and absorption wavelength [7]. Larger particle sizes results in that a bigger share of the

incoming light is scattered forward. Mie scattering is strongly dependent of the incoming light as $1/\lambda^2$. The skys appearance is an example of combined Rayleigh and Mie scattering where the shorter wavelengths of the light from the white light of the sun is scattered in the atmosphere making the sky appear blue.

2.5 Fluorescence

Absorbed light causing a molecule to be excited can be reemitted with a different wavelength resulting in fluorescence. This can occur in two ways, either as fluorescence or phosphorescence. In the fluorescence case a molecule is excited to a higher level where it looses energy due to a relaxation process and at the end it is deexcited thereby emitting a photon with a lower energy. The losses during the relaxation process is a non-radiative decay. For the phosphorescence case intersystem crossing occurs, meaning that the excited electron does a forbidden transition that could be a result from collisions. Usually the ground state is a singlet and if the molecule happens to be in a triplet state the deexcitation process will be relatively slow. The time scale for fluorescence deexcitation is around tens of nanoseconds while for phosphorescence the time scale is around milliseconds or longer. In Fig. 2.2 a transition scheme can be seen, showing possible transition and luminescence results.

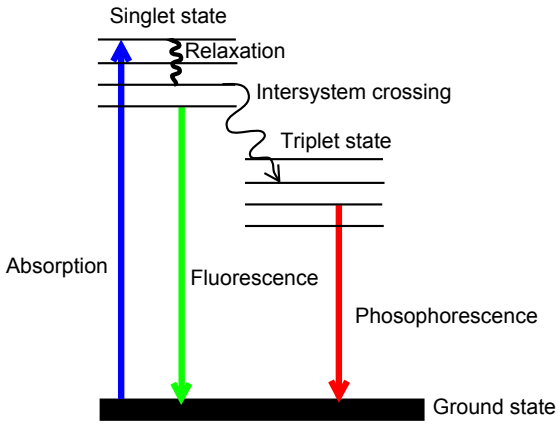

Figure 2.2: Simple Jablonsky diagram

The fluorescent light is normally Stokes shifted, i.e. the reemitted wavelength is longer than the absorbed. The loss of energy can come from collisions between molecules and excited state reactions.

Chapter 3

Present Techniques for Optical Property Determination

In this chapter an overview of techniques that are used today to measure optical properties will be given and problems with cross-talk will also be discussed. We will then proceed from the basic concept to the exact instrument. As mentioned before, measurements of the refractive index give an indication of the concentration of salt or sugar in a solution. The basic refractive index measurements are based on Fresnel's equations, evaluating the refracted light with regard to the incident. By comparing the polarization state and intensity the refractive index can be calculated [11]. The major problem with this method is that if the solution is absorbing light Fresnel's equations are unusable.

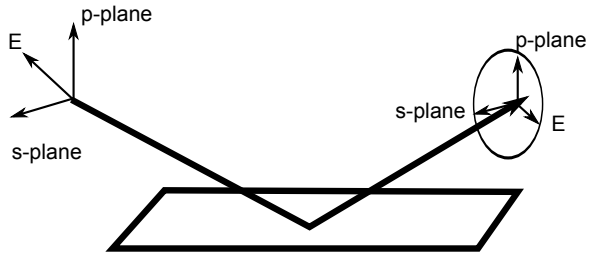

Figure 3.1: A schematic of the geometry of an ellipsometry experiment.

Another method of measuring the refractive index that is insensitive to absorbers is ellipsometry [12]. The principle of this method can be seen in Fig. 3.1. Light of a known polarization is transmitted on to a surface and

the polarization state of the reflected beam is measured. The polarization is measured with a quarter-wave plate and the relative amplitude Ψ and phase shift Δ are calculated from the measurements. Ellipsometry is a sensitive technique but time consuming, as it requires a scanning procedure for the quarter-wave plate and over a wavelength spectrum if that is wanted. Cross-talk will arise if the sample is turbid or a fluorophore is present in the solution.

Absorbance measurements are often conducted with the standard-addition method, where known concentrations are added to a sample resulting in an increasing concentration of the wanted measurable substance in the sample [13]. If the relation between the concentration and the measured unit is known, the original concentration can be extrapolated. For absorbance measurements the relation is given by the Beer-Lambert law, Eq. 2.2. Just like ellipsometry this method is time consuming because adding new concentrations takes time and the method is sensitive for cross-talk. If the sample is placed in a cuvette some of the light will be reflected at each surface where there is a refractive index difference. The result will be that the intensity measured will not only depend on the absorption, but also on the refractive index of the sample.

Another method to measure the absorbance and scattering is the time-of-flight method [14] [15], which is a good method if there is cross-talk between the absorbing sample and scattering. Scattering will result in unknown path lengths for the light. In time-of-flight spectroscopy the time for each photon to pass through the sample is known and thereby the effective path length, removing that unknown variable from the measurement. The disadvantage of this method is that the cost of the equipment is high as well as that it is time consuming method.

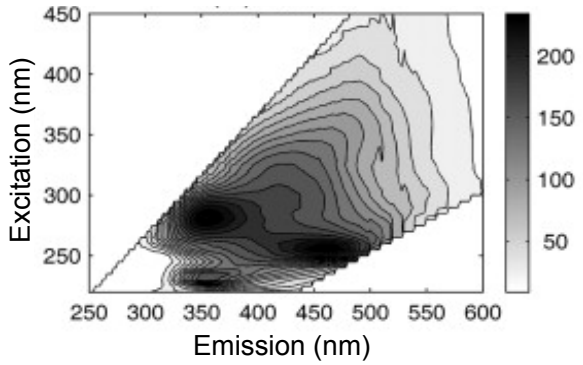

Figure 3.2: Typical contour plot of an EEM. From [16].

Fluorescence measurements are of great use when trying to analyze a sample. One type of fluorescence measurements is the use of an emission-excitation matrix (EEM) [17]. In the EEM a surface plot is produced by plotting the measured intensity against the excitation wavelength and emission wavelength. If no fluorophores are present the surface plot will be a diagonal line where the exciting wavelength will only generate the same emitted wavelength. For a substance with fluorescence the result will be that an excitation wavelength will yield longer emission wavelengths, corresponding to the upper half of the EEM shown in Fig. 3.2.

The integrating sphere method is an experimental setup that is used to determine optical properties of a sample. The three-point integrating sphere is used to determine the absorption coefficient μ_a, scattering coefficient μ_s and the anisotropy factor g. In the three-point method the setup consists of a sphere covered with a substance with high reflective properties, e.g. barium sulphate, and a part that allows for a collimated transmittance measurement [18], as seen in Fig 3.3. Collimated transmittance is the light that passes straight through a sample without scattering. By placing a sample at position 1 and 2 the total transmittance and diffuse reflectance of the sample can be measured. Position 3 is where the sample is placed when the collimated transmittance measurement is done. The integrating sphere method has also been used to measure optical properties of flowing blood [19].

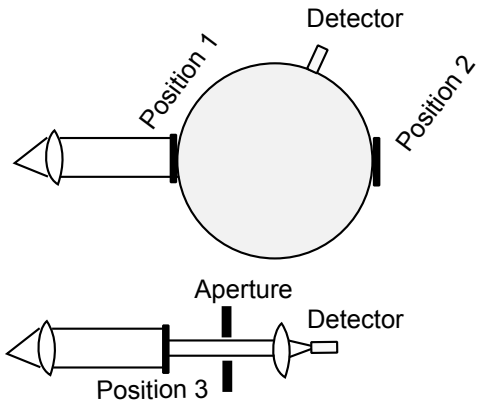

Figure 3.3: The three-point integrating sphere setup. Lower part is used for collimated transmittance measurements.

Interstitial photodynamic therapy (IPDT) is a method that can be combined with dosimetry. Then the optical properties in a whole tissue sample are determined by combining different optical paths between fibers [20] [21] [22]. This method resembles the one developed in this work with respect to combining light paths. By inserting fibers mounted in a special pattern with known path lengths between the fibers a combination of measurements can be done by sending a light pulse through one of the fibers and then detecting the response from the other fibers.

Chapter 4

Multivariate Analysis

In this chapter the method for analyzing the measurements acquired from the instrument designed in this paper will be discussed. The method used will be singular value decomposition (SVD) that is a common method for analyzing multivariate data. A mathematical introduction and explanation will be given as well as examples of the method. Singular value decomposition resembles principal component analysis (PCA).

The principle of PCA is to reduce the amount of variables on which a data set is dependent. By reducing the variables the data size is decreased and the data analysis is simplified. The basic idea of PCA is to find artificial variables for a data set which contribute to the largest variances in the data and thereby reducing the dimension of variables of the problem. These artificial variables are called principal components.

A common mis-interpretation is that the new variables after a PCA are fewer than before, when the number of variables are actually the same. The variables will decrease in significance as the variance for each new variable is smaller than the previous one, which will allow for an omission of variables with the smaller variances. Some information will be lost in this process as some variables are removed but that is often negligible. These components could also be noise in the measurement which in the decomposition will be separated from the data. PCA and SVD are well suited for analysis of data sets, where there may be a correlation between some of the variables as redundant variables can be replaced with fewer ones.

4.1 Basic statistics

Here will follow an introduction to the basic statistical knowledge needed to understand PCA. In the following chapter it is assumed that there is a

known data set, and a sample of that set is called X. The variance for a data set is the average difference for each number in the set from the mean value. If a sample of the data set is X then the variance is given by

$$\sigma = \frac{\Sigma_{i=1}^{n}(X_i - \overline{X})^2}{n-1}, \tag{4.1}$$

where $\overline{X}$ is the mean value of the sample. The variance is the square of the standard deviation. The variance is used for one-dimensional data sets. If the data set has more than one dimension it could be useful to see if the dimensions correlate in some way or other. The covariance is one measure of the correlation between two dimensions and is given by

$$\sigma = \frac{\Sigma_{i=1}^{n}(X_i - \overline{X})(Y_i - \overline{Y})}{n-1}, \tag{4.2}$$

where X and Y are two different dimensions of the data set. The reader is assumed to have basic knowledge of matrix computations such as eigenvector calculations and eigenvalues.

4.2 Singular value decomposition

For the mathematical explanation of singular value decomposition, assume that there is a matrix $\mathbf{X}$ which has the dimensions $(n \times p)$. n is the number of observations and p the number of observed variables. The singular value theorem states that a matrix $\mathbf{X}$ can be decomposed in three different matrices according to Eq. 4.3 [23].

$$\mathbf{X} = USV' \tag{4.3}$$

U and V are orthonormal matrices with the dimensions $(n \times r)$ and $(p \times r)$, respectively, and S is a diagonal matrix containing the singular values. Depending on the application that SVD is used for, U and V get different interpretations. In spectroscopy, for example, the U matrix can describe so called base spectra if the spectral components are in the n direction of $\mathbf{X}$. A measured spectrum can be constructed by combining the different base spectra with varying weights. The first base spectrum is the one that accounts for most of the variation in the measurements. The last base spectrum accounts for the smallest variation which allows for possible truncation and thereby reducing the data. Truncation means that base spectra that have no significant influence on a constructed spectrum are removed.

One way to see how many base spectra that are needed to construct a good realization of a real spectrum is to look at the singular values in

the S matrix. The singular values decrease in magnitude for each step and can be interpreted as how much influence each base spectrum has on the measurements. Depending on how many variables that are involved in the measurements a different number of singular values are needed. One singular value can be a combination of different variables; 75% of something and 25% of something else. Fig. 4.1 shows a plot of singular values.

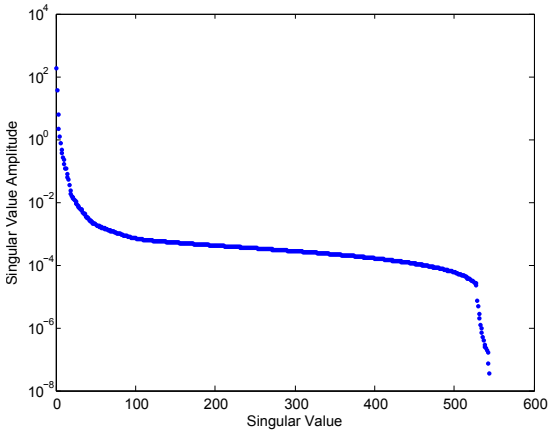

Figure 4.1: An example plot of singular values from a decomposition done from a measurement in this thesis. The last drop in amplitude could come from outliers in the measurement.

It can be seen that there are two different slopes; one slope in the beginning for the first singular values and and one for the rest. For the last singular values there can be a big decrease in value as seen in Fig. 4.1. This could mean that there are either duplicate measurements or measurements that are differing a lot from the other measurements, called outliers.

A practical example of how the SVD works will now be explained. Assume measurements of a sample generate a spectrum seen in Fig. 4.2 depending on the concentration the intensity will vary. A substance is added to the sample which gives rise to a peak such as the one seen in Fig. 4.2. A range of measurements is done with different concentrations of the added substance. The data are analyzed using singular value decomposition, where two singular values can be seen to affect the measurement the most and which have the corresponding base spectra seen in Fig. 4.2. One for the original sample and one for the added solution. By using a different weights of the second base spectrum the peak arising from the added solution can be imaged for different concentrations. Normally the base spectra can have negative intensities and a physical explanation can be difficult to make.

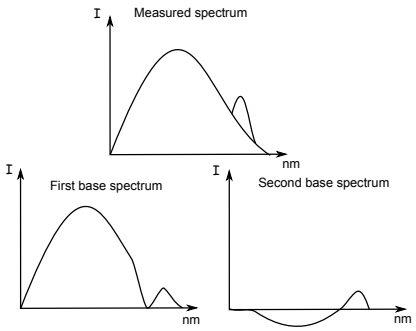

Figure 4.2: Shows an idealistic case of singular value decomposition where a measured spectrum has been decomposed in two base spectra.

Chapter 5

Semiconductors

Semiconductors are of a great importance in this paper, since light emitting diodes (LEDs) are the light sources used for the measurements, and photodiodes are used to detect the response from the liquids. In this chapter a detailed analysis of the physics behind these two semiconductor components will be discussed. There will also be a discussion of what affects the efficiency of the LED and how this can be controlled to achieve a good light source for the instrument constructed in this work.

5.1 Light emitting diodes

A semiconductor has a bandgap that differs in size depending on the material. In Fig. 5.1 a simple visualization of a semiconductor can be seen. In the lower state (conduction band) electrons are situated and in the upper states (valence band) holes. The holes and electrons can recombine resulting in a lower energy for the combined parts. As the energy has to be conserved the extra energy can be released as a photon or in form of a phonon. If all the energy goes to the photon the energy gained will be equal to the size of the bandgap. When a photon is released it is called radiative recombination. When no photon is released it is consequently referred to as non-radiative recombination. The result of non-radiative recombination is vibrations in the crystal structure of the semiconductor, i.e. heat. For LEDs it is desired to minimize the amount of non-radiative recombinations for obvious reasons [24].

A semiconductor can be doped in two ways. Doping means creating an excess of carriers, either holes or electrons, which is introduced in a semiconductor. P-doped semiconductors have an excess of holes and n-doped an excess of electrons. The amount of light from the LED is determined

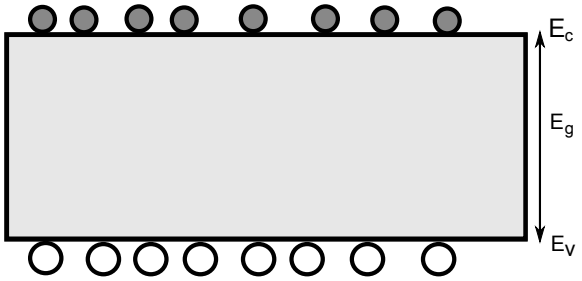

Figure 5.1: A visualization of a semiconductor. E_c is the conduction band where the holes are located and E_v is the valence band where the electrons are. E_g is the bandgap.

by the recombination rate. The recombination rate is proportional to the concentration of holes and electrons and is given by the Eq. 5.1.

$$R = Bnp, \tag{5.1}$$

where B is the bimolecular recombination coefficient and n and p are the electron and hole concentration, respectively.

Several physical phenomena can give rise to non-radiative recombination. The most common cause is imperfections in the crystal structure such as atoms of the wrong type, native defects and dislocations. The native defects can introduce unwanted energy levels in the bandgap of the original semiconductor. These energy levels will cause the recombination to go through extra steps in the original bandgap resulting in a non-radiative recombination.

The temperature dependence of what type of recombination that occurs is given by the material the semiconductor is made of. It can be shown that the non-radiative lifetime of recombination decreases with increasing temperature according to Eq. 5.2 which gives the lifetime for holes and electrons for intrinsic materials [24].

$$\tau_i = \tau_{n0}\left(1 + \frac{p_1 + n_1}{2n_i}\right) = \tau_{n0}\left[1 + cosh\left(\frac{E_T - E_{Fi}}{kT}\right)\right] \tag{5.2}$$

E_{fi} is the intrinsic Fermi level,τ_{n0} is the lifetime for electrons, k the Boltzmann constant and T the temperature. Higher temperatures will result in shorter radiative recombination lifetimes. Some semiconductors uses materials with deep states for recombination which with increased temperature will increase the efficiency of the semiconductor.

A semiconductor that requires both a photon and a phonon for recombination is called an indirect bandgap semiconductor. A phonon is the quantization of vibrations that may occur in a semiconductor. These semiconductors benefit from higher temperatures as phonons are more common and thereby simplifying the recombination process.

It is possible to reduce the defects in a semiconductor but it is impossible to remove them completely. There will always be some surface, Auger and Shockley-Read recombination. The amount of photons generated in the total recombinations is given by the internal quantum efficiency, Eq. 5.3, and is a measure of how efficient the LED is. Some of the LEDs of today can have an efficency of more than 99% [24]. This has some interesting effects on LED intensity. E.g, the efficiency of an LED changes from 80% to 90% which results in that the generated heat from the current is halved. This means that the current can be increased two times without destroying the LED. The intensity is increased both from the higher efficiency and the increased current resulting in an increase in intensity with a factor of 2.25.

$$\eta_{int} = \frac{\tau_r^{-1}}{\tau_r^{-1} + \tau_{nr}^{-1}} \tag{5.3}$$

LEDs are constructed with a combination of n- and p-doped materials, called a p-n junction. The simplest p-n junction consists of two differently doped materials next to each other. In the region where the materials meet, holes will start recombining with electrons. This results in a region with no carriers called a depletion zone. As there is an abundance of electrons on one side of the zone and holes on the other side, an electric field will be created stopping further carriers to move to the other side to recombine. The electric field is known as the diffusion voltage and is calculated from Eq. 5.4.

$$V_D = \frac{kT}{e} ln \frac{N_A N_D}{n_i^2}, \tag{5.4}$$

where N_A and N_D are the dopant concentrations and n_i is the intrinsic carrier concentration. The voltage over the depletion zone can be either increased or decreased by applying a backward or forward bias, respectively. For forward bias the current increases as carriers are forced into a region with opposite charge carriers. In Fig. 5.3 the relation between the voltage and current for a LED is be seen.

The bandgap has been marked in Fig. 5.3. At this voltage the current increases strongly for different voltages and the dependence can be assumed to be linear. The bandgap can be calculated from the plot given in Fig. 5.3.

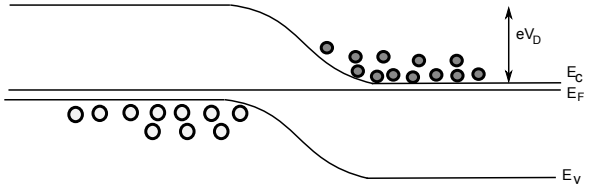

Figure 5.2: Schematic over a basic pn-junction.

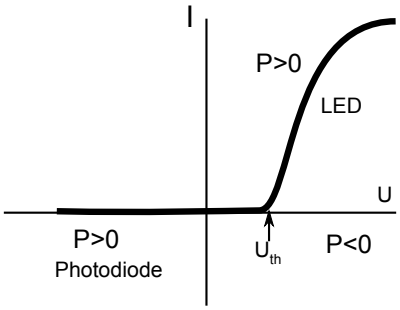

Figure 5.3: The dependence between the current and voltage for an ideal diode. Two different regions where the diode is an emitter and a detector has been marked. P is the dissipated power $P = U \cdot I$.

From Fig. 5.2 the following equation can be acquired.

$$eV_D - E_g + (E_F - E_V) + (E_C - E_F) = 0 \tag{5.5}$$

As the separation between the conduction band or valence band and the Fermi level is very small for highly doped materials, which in the case for LEDs, the third and fourth term can be neglected. This results in that the band gap is equal to the diffusion voltage which is equal to the threshold voltage.

$$E_g \approx V_D \approx V_{th} \tag{5.6}$$

By measuring a few value combinations of the voltage and current in the linear region for a LED the bandgap can be calculated by extrapolating the values to acquire the threshold voltage. In some cases LEDs can be turned on before reaching the turn-on voltage due to carrier transport through deep levels in the bulk or through surface states. This is called sub-threshold turn-on.

The efficient high-intensity LEDs that are used today are often constructed from a heterojunction. In Fig. 5.2 a homojunction can be seen.

A heterojunction is made from two different semiconductors, one with a small bandgap and the other one with a large bandgap. In the heterojunction a higher concentration of carriers is acquired in the region where small bandgap material is located. This is due to the fact that the limitation of the zone where recombinations occur is given by the width of the small bandgap layer instead of the diffusion length as in homojucntions. From the above it is known that the intensity is proportional to the recombination rate. In turn the recombination rate is proportional to the carrier concentration.

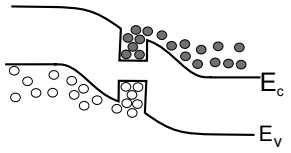

Figure 5.4: Heterojunction for a light emitting diode.

LEDs will be saturated at high enough currents causing no increase in intensity even if the current is increased even further. This saturation occurs in heterojunctions when the current is high enough so that the Fermi level is above the barrier. This means that an increase in current will still result in the same concentration of carriers in the active region. When doing measurements of different intensities for the LED this has to be taken in consideration as the current may increase but the intensity stays the same, which could result in erroneous conclusions.

The intensity profile of an LED is given by Eq. 5.7.

$$I(E) \propto \sqrt{E - E_g} * e^{-E/(kT)} \tag{5.7}$$

and is acquired by calculating the density of states and multiplying it by the distribution of carriers from the Boltzmann distribution. Peak intensity is $E = E_g + \frac{1}{2}kT$. It should be mentioned that many of these theoretical equations, that for example describe the emission spectrum can be a bit off in reality. The emission spectra should have a sharp cut-off wavelength to longer wavelengths due to the square root, but in reality this is not the case.

An issue to consider is that the spectral characteristics of an LED changes with temperature and the LED can even break if the temperature becomes too high. This could, for example, happen when too high currents are used. In this work currents exceeding the specified limit are used to achieve higher luminosity. To avoid destroying the LEDs they are made to blink at a high frequency, limiting the time when the LED is lit up.

$$dT = c^{-1}(P_{in} - P_{out}) = c^{-1}(U \cdot I - P_{em} - P_{heatcond.} = c^{-1}(U \cdot I(1-\eta) - P_{heatcond.}) \tag{5.8}$$

Eq. 5.8 shows a simplified equation of the temperature variations in a LED. c is a temperature coefficient U the applied voltage, I the current, η the quantum efficiency, P_{em} the effect lost due to light emission and $P_{heatcond.}$ the heat lost due to heat conduction.

5.2 Photodiodes

Photodiodes are detectors made of semiconductor materials in a pn-junction arrangement just as light emitting diodes. To improve the response time of the photodiode, intrinsic semiconductor material may be inserted between the p- and n-doped layers. These photodiodes are called PIN diodes. The PIN diodes are well suited to use in optical system where a fast read off is necessary.

There are two operational modes of a photodiode, the photovoltaic mode and the photoconductive mode. In Fig. 5.2 the dependence of current and voltage for a photodiode can be seen. The two different operational modes are noted in the figure. In the photovoltaic mode incoming light generates a voltage. This mode is not the optimal detection mode as the response from the incoming light is non-linear which can be seen in the figure. Solar cell operate in the photovoltaic mode.

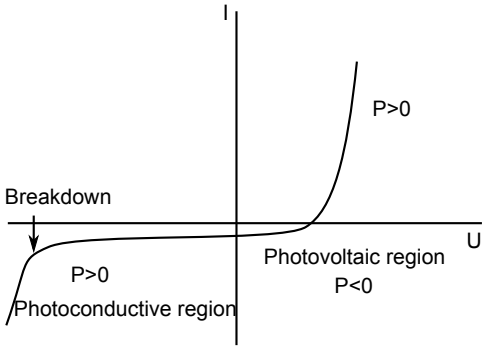

Figure 5.5: The dependence between the current and voltage for a diode. P is the dissipated power $P = U \cdot I$.

In the photoconductive mode the photodiode is exposed to a reversed bias. The resulting current is proportional to the incoming light intensity.

The advantage of this mode is that it has a faster response time due to decreased capacitance from the reverse bias as well as that the generated current is linearly proportional to the incoming light. However, the drawback is that the noise is higher in this mode.

Photodiodes have some important properties which should be taken into consideration when choosing a detector for optimal performance. The responsivity is a measure of how well the detector generates a current depending on the incoming light. The responsivity is given by $R = \frac{\eta e}{h\upsilon}$ where η is the quantum efficiency. The quantum efficiency is a measure of how many photons contribute to the detected current. This value is dependent on temperature which makes the responsivity temperature sensitive. The response speed of the photodiode is another important property that determines the rise and fall time of a detector.

Another important problem to consider in the detection scheme is the time/gain dilemma of the photodiodes. This dilemma can be seen, for example, when a pictures is taken with a camera. Either a long exposure time can be used and a good picture acquired with the disadvantage of bad temporal resolution, or a short exposure time resulting in a worse picture but with a better temporal resolution.

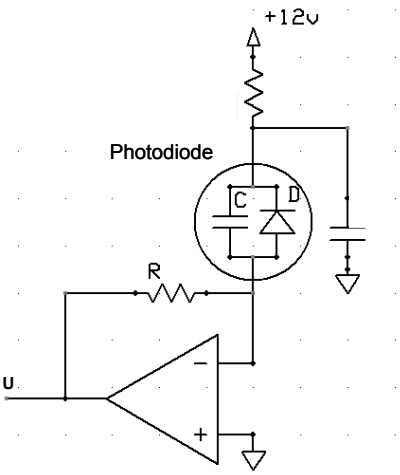

Figure 5.6: Amplifying circuit of a photodiode. Measured voltage $U \propto -I_{pd} \cdot R$.

The photodiode is connected in an amplifying circuit where the dimension of the detected signal is proportional to a resistance. A larger resistance yields a better signal detection. The time dilemma is introduced because the

photodiode is constructed with an internal capacitance. As the resistance and capacitance are coupled in series, the time response of the system will increase with an increased resistance. Fig. 5.6 shows the amplifying circuit. A backward bias will decrease the internal capacitance to a certain degree until the photodiode breaks from a too high bias.

The noise of a detector introduces disturbances to the measured signal. If the noise is too large the signal can be distorted and the result can be impossible to distinguish. For a photodiode there are mainly two types of noise, shot noise and thermal (Johnson) noise. The shot noise is given by $I = \sqrt{2q(I_p + I_D)f}$, where I_p is the generated current, I_D the dark current and f the noise measurement bandwidth. Thermal noise occurs because of the generation of free carriers due to heat.

Chapter 6

Method

As previously mentioned there can be many variables when determining the optical properties of a liquid, such as absorption, scattering and fluorescence to say a few. There is also the cross-talk between the properties that further increases the difficulty to measure the properties of liquid solution. In this chapter the method for determining the optical properties will be described. The measurement system construction is discussed. Further, it is described how the data are acquired and analyzed.

The design of the instrument is of great importance when trying to measure the optical properties of a liquid, especially so when determining all of them simultaneously. This requires that the instrument is constructed in such a way that it is able to detect all the different optical properties during the same measurement. Another issue to consider is the difference in optical properties for different wavelengths as well as for different temperatures. As there are a lot of variables to determine, many measurement values are needed to create an equation system with a specific solution. In the following section, the considerations when designing and constructing the instrument are given. The construction will first be explained and then how this allows for measurement of the different optical properties.

6.1 Instrument construction

The basic principle of the instrument is to let a liquid solution flow through a transparent tube and let light emitting diodes shine on the liquid and then detect the response with photodiodes after the light has passed through the liquid. The tube is mounted in a copper bar with a hole drilled right through it. The copper bar also has holes drilled for the light emitting diodes and photodiodes. The copper bar contributes to some stability in

the measurements such as a homogenous temperature distribution for the bar which is an important feature for the mounted LEDs and photodiodes as their emissive yields and response vary with the temperature. The bar reduces fast temperature variations in the system. For further temperature control Peltier elements could be fastened to the copper bar. This would allow for specifically choosing the temperature of the bar independent of the temperature of the room and liquid.

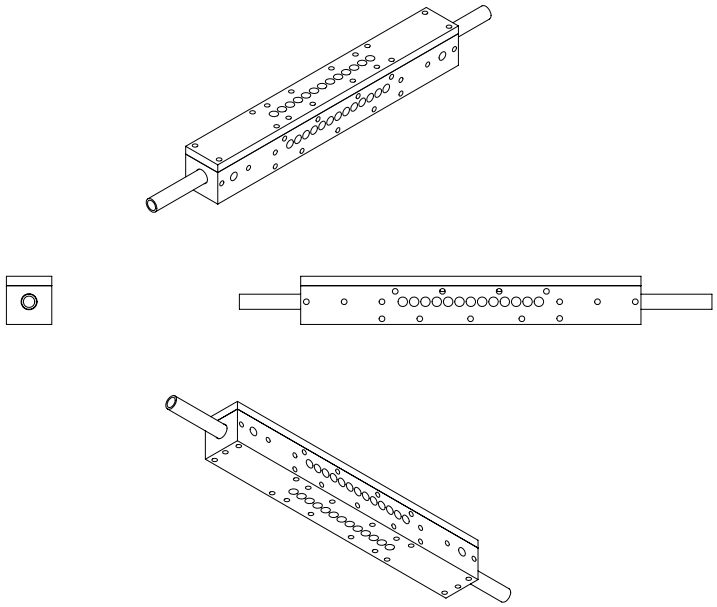

Figure 6.1: Overview of the copper bar.

Another thing to consider in the mounting process is the surface on the copper bar just outside the tube. The surface will affect the ability to determine the optical properties whether it is absorbing or reflecting. A reflecting surface will allow for more light to be detected. In the setup used for the measurements in this work there were no alterations to the surface, the regular copper surface. Fig. 6.1 shows how the copper bar is constructed.

The tube through which the liquid solution is flowing has to be transparent for whole the wavelength region utilized in the setup. Quartz is a material with suitable properties as it transmits light between 0.2 to 2 μm

and it is sturdy enough to withstand the possible small forces that could be applied to the tube during a measurement procedure. The surface of the tube will affect the measurements. It can either be a clear surface or have a scattering surface called blasted. The blasted surface will contribute to scattering the light along the tube which means that for non-scattering liquids detectors far from the source will still be detecting a signal and thereby increasing the measurement values. On the top of the copper bar there is a removable lid used for mounting cut-off filters in front of photodiodes. The cut-off filters are used to filter out all of the light from the LED opposite of the filter and most of the light from the neighboring LEDs. This is done so that fluorescence can be detected without influence from the excitation light. What has to be taken into account is that the filters themselves can fluoresce and disturb the measurement.

6.1.1 Illumination and detection

As seen in Fig. 6.1 there are thirteen larger holes drilled on each side in the middle of the copper bar. On two of the sides mounted perpendicular to each other are two circuit boards, each with thirteen light emitting diodes. On the other two sides there are circuit boards mounted with photodiodes as detectors. In front of one of the detector boards there are cut-off filters, filtering the light from the LED placed at the same position as the detector. There are only seven detectors that are used in this way and they are all situated at the same position as the seven lowest wavelength LEDs. These detectors are used to detect the possible fluorescence induced by the LEDs.

On the other detector board there are so called elastic diodes optimized for detection of light of the wavelength of the LED on the same position as the detector. Using many detectors is advantageous because it allows for the use of many different detector materials making the setup able to detect light of a wider wavelength spectrum than if only one detector type was used, from UV-enhanced silica for ultra-violet light detection to InGaAs detectors for detection of infrared light.

The thought behind using light emitting diodes as light sources is to be able to illuminate the liquid solution with different wavelengths and detect the specific responses. A light emitting diode is a suitable light source because of the specificity of the wavelength (around 10 nm spectral width) and the fast response time. Why the fast response times are wanted will be explained in the next section. In Table 6.1, the peak wavelengths of the LEDs used in the instrument are listed. The reason why there are 15 LEDs but only 13 holes is that two of the LEDs are double banded meaning that they

have two different wavelength bands that can be controlled independently. The z-position given in the table indicates at what position each LED is placed. The z direction is in the direction of flow of the liquid solution. In Fig. 6.1 the z direction in the middle right figure is to the right.

Z-position	Wavelength [nm]
1	1700
2	1300
3	1200
4	1070
5	940
6	850
7	700
7	760
8	660
8	591
9	528
10	477
11	432
12	395
13	355

Table 6.1: Peak wavelength of the LEDs used in the instrument.

To summarize the resulting light paths of the illumination and detection configuration the amount of measurement values is equal to the number of LEDs multiplied with the number of detectors. There are some restrictions to this argument as the sensitivity region of the detectors varies a lot, meaning that detectors optimized for near-IR light will have low sensitivity for UV light. This combined with a long path length from the UV LEDs to the IR detectors will result in a small detected signal. Disregarding those circumstances the number of measured values can be calculated. Since there are eleven broadband photodiodes and seven fluorescence detection photodiodes there are a total of $30 \cdot 18 = 540$ unique light paths.

6.1.2 Multiplexing

During a measurement only one light source should be lit up at one moment or the detected signal from a photodiode will detect a possible mix of intensities from the different light sources which will result in a faulty

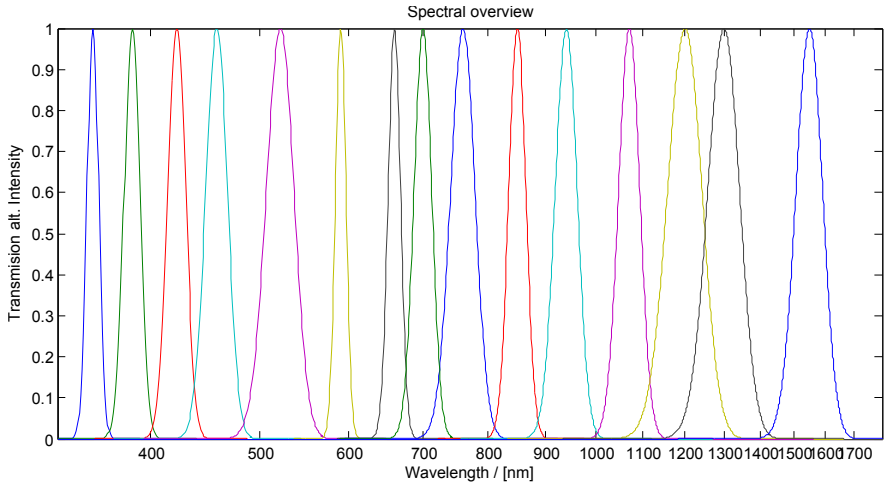

Figure 6.2: The spectral bands of the instrument. (Courtesy of Mikkel Brydegaard)

measurement value. To solve this problem a counter circuit consisting of two 4-bit counters [CD40193be] is introduced and connected to the two LED boards. The counter receives a digital pulse train from a pulse generator. The counter has four output pins that can either be logically true or false (high or low voltage) and changes for every pulse received from the pulse train. The first counter is directly connected to the pulse train and the second counter is connected to the carry of the first counter. The carry changes between true and false every time the counter has counted all the bits, in this case after 16 pulses. This means that the first output of the second counter will vary between true or false every 16 pulse. This pin is used to control which of the two boards will shine. The first counter is connected to a demultiplexer [CD4514], one on each LED board.

The demultiplexer receives a 4-bit input signal and converts it to a high voltage signal on one of the 16 output pins. The output signal for every output pin is each connected to a transistor that in its turn controls a LED except for one of the transistors that controls a resistor. In this way the LEDs can be made to blink at a specific frequency depending on the frequency of the pulse train. An important quality of the LEDs is that they have a fast response (rise) time allowing for faster blinking and more measurements to be done during a set time interval.

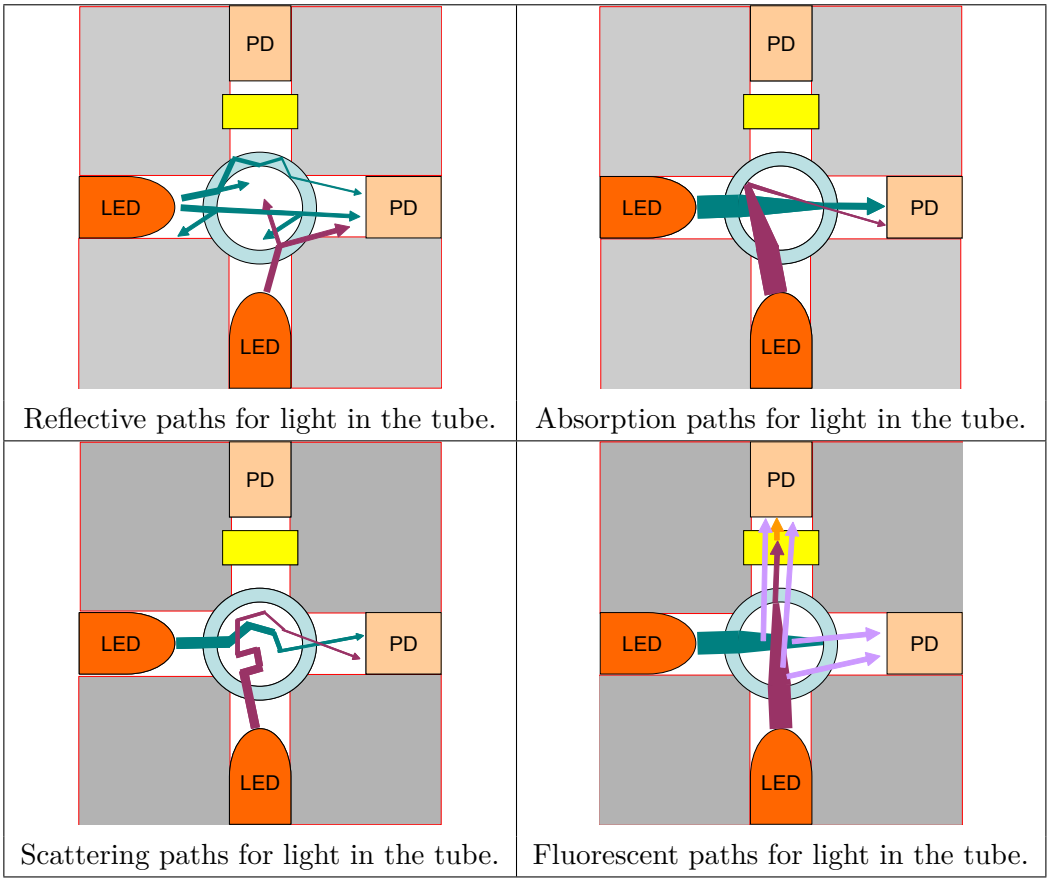

Reflective paths for light in the tube. | Absorption paths for light in the tube.

Scattering paths for light in the tube. | Fluorescent paths for light in the tube.

Table 6.2: Cross section of the copper bar in the X-Y plane. (Courtesy of Mikkel Brydegaard)

6.2 Combinatorial light paths

In this section an explanation of how all the optical properties are possible to be measured from the special construction of the instrument will be given. As has been mentioned, the ability to determine the properties comes from acquiring a lot of measurement values and creating an overdetermined system. In Tab. 6.2 the four possible direct light paths for every z-position can be seen, detection of transmitted light, laterally scattered light, laterally scattered fluorescence and straight forward fluorescence.

Table 6.3 shows how the light is detected at detectors not only opposite of the shining LED but also at other z-positions.

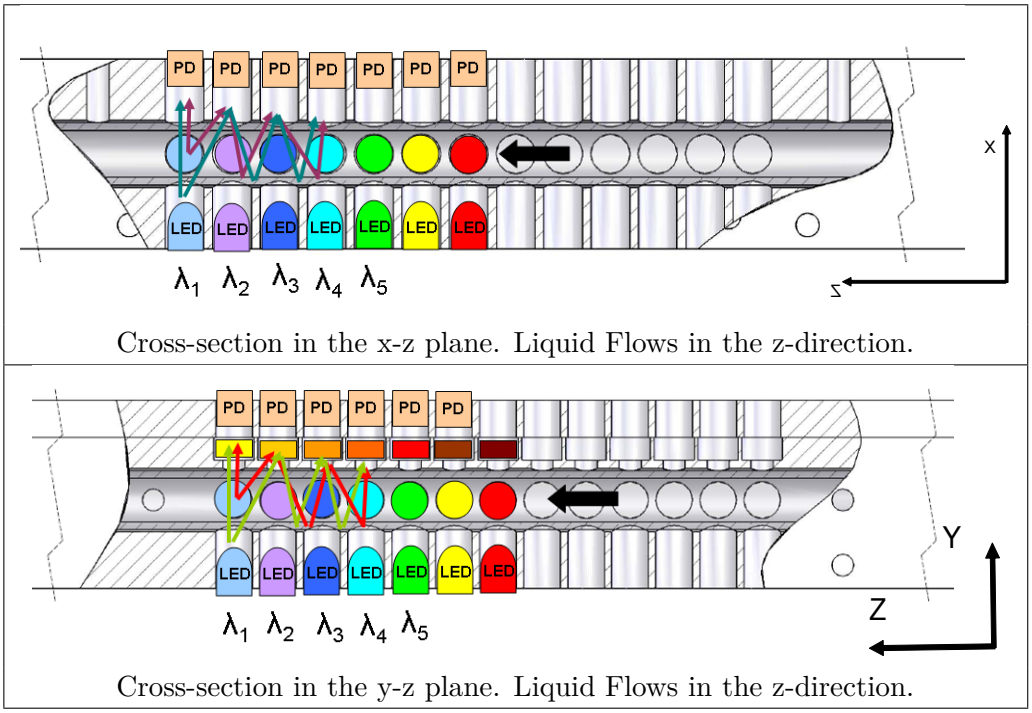

Cross-section in the x-z plane. Liquid Flows in the z-direction.

Cross-section in the y-z plane. Liquid Flows in the z-direction.

Table 6.3: Cross section of the copper bar in the X-Z and Y-Z plane. (Courtesy of Mikkel Brydegaard)

6.3 Data acquisition

The data are gathered by using a National Instruments Data Acquisition Card (DAQ). In the specific setup used in this work a NI DAQ 6218 was used. The data consist of voltage readings from photodiodes that are proportional to the intensity. The measurements are done with a single-ended reference, meaning that a common ground is used for all photodiodes. The 6218 has a maximum sample speed of 250 kS/s (kilosamples/s) resulting in a maximum of $250/18 \approx 14$ kS/s if all 18 channels are measured simultaneously. The sample speed can be increased by not measuring all the channels simultaneously. During the measurement, five channels where sampled simultaneously acquiring 15 kS for every channel per measurement equalling a sampling speed per channel to 50 kS/s.

A clock pulse connected to the counters is generated by the DAQ card with a maximum frequency of 80 MHz. The measurements done in this work uses a clock pulse frequency of 4 kHz giving a LED frequency of $4000/32 = 125$ Hz. Every LED is thereby lit up for 8 ms at a time. The five channels are measured during a time span of 0.3 s resulting in that each LED is on

$0.3/0.008 = 37.5$ times for each measurement.

Two digital output channels are used to control the intensity of the LEDs by changing the current to the LEDs. There is a constant current circuit where the voltage is dependent of the bandgap of the LED that is on. The readings from this is called the common anode. A bigger bandgap gives a higher measured voltage. A typical plot of the common anode is seen in Fig 6.3. Every time an LED is on, approximately 14 samples are acquired. For every signal approximately $14 \cdot 37 = 518$ measurement values are acquired with leads to a good signal-to-noise ratio because of averaging. Also the variation between measurements of the same liquid are small which will be shown in Chap. 7.

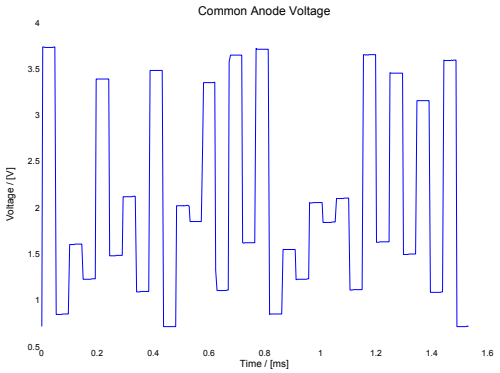

Figure 6.3: Common anode signal.

By measuring the voltage over the LED for different currents an I-U plot can be constructed as mentioned in Sect. 5.1. By extrapolation of this plot the bandgap and thereby the wavelength of the LED can be acquired. Due to some electrical construction issues the voltage measured from the common anode is not the exact voltage over the bandgap but also includes some other electrical components which makes the calculation of the bandgap faulty. As the wavelength of the LEDs are known as well as the order in which they blink this was not an issue during the measurements done in the laboratory. The wavelength of each LED was investigated using a spectrometer and the wavelengths were found to match those, stated in the specifications.

6.3.1 Temperature calibration

As stated in Chap. 5.1 the emissive yield (LED) and quantum efficiency (PD) varies depending to the temperature. During a measurement this has to be considered when measuring on a liquid whose temperature differs from

the room temperature. The heat transfer between the quartz tube and the copper bar is rather good which will cause temperature changes in the copper bar depending on the temperature of the liquid. As the copper bar temperature changes, so will the properties of the LEDs and photodiodes too. There are a couple of ways to solve this dilemma; either try to stabilize the temperature of the copper bar using external Peltier elements or measuring the change in illumination and detection problem and compensate for it. The disadvantage with using Peltier elements is the difficulty to stabilize the temperature because of the size of the copper bar and the lack of space to mount the elements due to the different circuit boards. Whereas the liquid can easily change the temperature of the bar, the elements take considerably more time to compensate for it.

Instead of using Peltier elements, the method used in the measurements in this report uses known light responses for the LEDs and photodiodes and compensates for the difference. A measurement is done, where the temperature is changed from low to high and measuring the response of each photodiode for every LED, meaning that $18 \cdot 30 = 540$ curves are acquired. A regression curve is fitted to every measured curve. The temperature for each measurement is recorded using two thermocouples that are mounted inside the copper bar. In the calibration made in this report the temperature was changed from 10^o C to 35^o C and the temperature variation (thermocouple voltage) dependent on the time can be seen in Fig. 6.4.

6.3.2 Data analysis

In this section the general form of the data analysis will be disclosed. Depending on the measurement, different variables have to be taken into account, e.g. different normalizations which will be described in the specific measurement.

There are four different data sets that can be chosen for each measurement, one for every current selection. For liquids with high absorbance a higher intensity of the LEDs could be needed to be able to acquire a good signal at the photodiodes. For low absorbing liquids some detected signals can be saturated to have the same value as the voltage supplied to the operational amplifier. When measuring on these kind of liquids it is more suitable to use one of the lower currents. In scattering liquids an increase in intensity of the LEDs will yield more light to photodiodes further away from the LED but at the same time a saturation effect of a close lying photodiode can be achieved.

During the data analysis a temperature compensation is also performed.

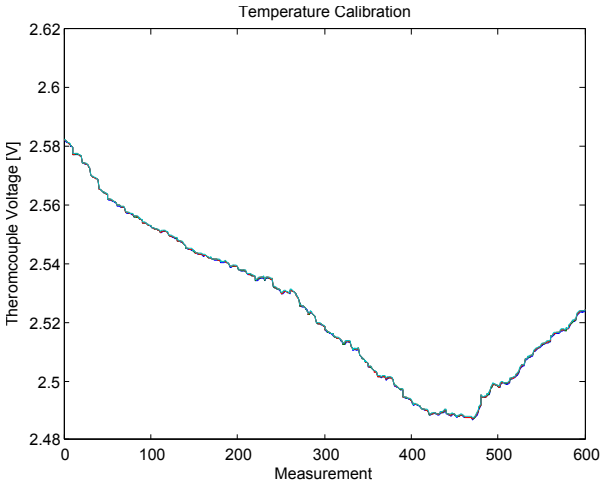

Figure 6.4: The temperature calibration used in all measurements for this work. The low voltages correspond to higher temperatures and vice versa. The temperature can be seen going from approximately 10^o C to 35^o C and then sink again.

A normalization temperature that lies in the interval of the temperature calibration measurement is chosen, and all values are normalized to that value. The dark current is also subtracted from the result. As was described regarding the construction of the instrument there is, on each LED circuit board, a resistance that is used to determine the dark current. This means that the response for two of the pulses in the 32 pulse interval is when no LED is lit up. Eq. 6.1 gives the resulting values that are used in the SVD.

$$I = (I_M - I_0) \cdot C_N, \tag{6.1}$$

where I_M is the measured values, I_0 is the dark current intensity measured and C_N is the normalization value that is equal to the ratio between the intensity for the temperature of the measured value and the intensity of the normalization temperature. A unitless data set can also be acquired by dividing Eq. 6.1 with a normalization intensity, for example a measurement of pure water.

After the preprocessing of the data is completed, SVD is performed. A rough validation of the SVD can be done by investigating the singular value plot. If there are two slopes of singular values as mentioned in the theory part the SVD can be considered somewhat successful. Erroronous measurement values can be detected in different ways. A so called scatter

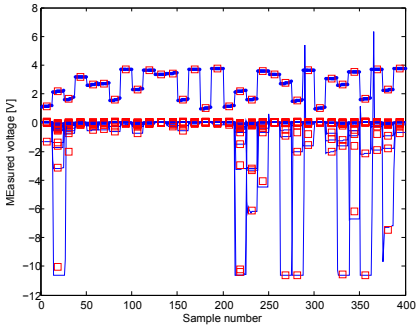

Figure 6.5: Example of a measurement acquired. The red squares signify the middle of the 32 plateaus of the upper curve and the voltages of the lower curves are extracted for these values.

plot, where columns from the matrix U in Eq. 4.3 are plotted against each other can be created. Deviant measurement values can be seen from the scatter plot as they differ from a pattern that the correct values follow.

After a measurement is done, a model is created so that future measurement values can be analyzed. Faulty measurement values have to be removed before processing or the model will also be faulty. The model is used for determination of concentrations of substances in an unknown sample. When creating the model a truncation is performed where only the significant singular values and corresponding base spectra are used. The model should strive to resemble the real problem. In the model used in this report a quadratic model with allowance for offset was used. This does not portray the real problem correctly as it is known that there are absorbing effects in the liquid making the intensity be exponentially decaying as in Eq. 2.2, meaning that in this case a quadratic curve is fitted to an exponential decaying one. Depending on the values of absorbance the quadratic curve could be fitted in the middle of the exponential curve resulting in a larger fault for predictions of rather high or low absorbance as seen in Fig. 6.6. A link function can be used to fit a linear model to a non-linear phenomena. The kind of link function that is used depends on the non-linearity. For the case in this work it is known that the intensity should decrease exponentially. A link function that will likely increase the model fit is therefore the natural logarithm (ln).

For the model to be able to predict concentrations it has to be trained. The training is done using the leave-one-out principle, which allows for the training to be instantaneously verified. When the measurement is done concentrations for each measurement are noted to be able to train the model

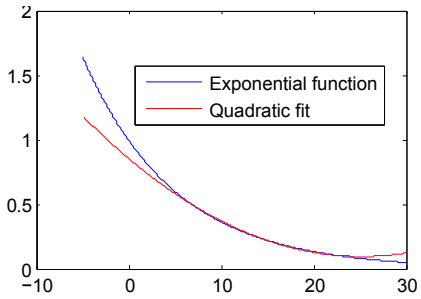

Figure 6.6: A quadratic fit of an exponential decaying curve.

afterwards. It can then be understood that to be to able determine specific concentrations of a substance in a liquid the instrument has to be trained first, i.e, measurements where the concentrations are known, have to be performed before measuring on unknown samples.

In the leave-one-out training a model is created using all but one of the measurement values. The model is verified by trying to predict the value that was left out with the model and compare it to the real value. This is then done for all the measurement values and a good indication of how well the model works is given by comparing the real and predicted values. The difference between a fitting model and the leave-one-out prediction model is that a fitted model gets better when more information is take into account. For the leave-one-out model the prediction is better up to a certain truncation but is then worsening since the system becomes unstable; Fig. 6.7. Another disadvantage with the leave-one-out is that it requires a lot of computational power as the training has to be done once for every sample.

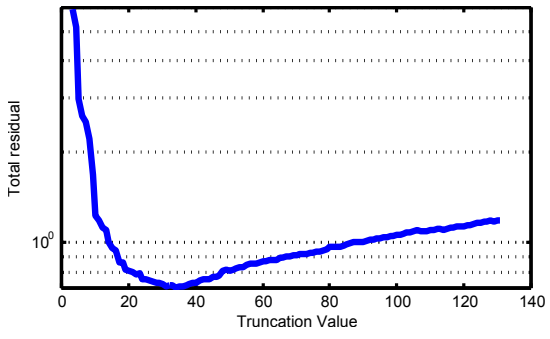

Figure 6.7: The logarithm of the residual plotted against the truncation number.

The training is practically done as explained here. Assume a measurement M where the rows are the number of measurements n and and the columns k the number of measurement values, in this case 540 for every measurement.

$$M = \begin{bmatrix} x_{n=1,k=1} & \cdots & x_{n=1,k=540} \\ \vdots & \ddots & \vdots \\ x_{n,k=1} & \cdots & x_{n,k=540} \end{bmatrix}$$

For every measurement n there is a corresponding known concentration given by Y. j is in this case the number of different substances added to the sample.

$$Y = \begin{bmatrix} y_{n=1,k=1} & \cdots & y_{n=1,j=5} \\ \vdots & \ddots & \vdots \\ y_{n,k=1} & \cdots & y_{n,j=5} \end{bmatrix}$$

A singular value decomposition is done of M according to Eq. 4.3. In this case the base spectra are in the U matrix. A truncation is performed with T truncation values and a model Ψ is created. In this case a quadratic model. The degrees of freedom of the model is given by the number of columns in the model, i.e. $1 + 2 \cdot T$.

$$\Psi = \begin{bmatrix} \vdots & \vdots & \vdots \\ 1 & U_{1..n,1..T} & U^2_{1..n,1..T} \\ \vdots & \vdots & \vdots \end{bmatrix}$$

A function Θ multiplied with the truncated model should yield the correct concentrations $Y = \Psi \cdot \Theta$. The problem is that Θ is unknown. To acquire Θ the leave-one-out method is used. This results in the function $\hat{\Theta} = \Psi \backslash Y$ where one measurement is left out for validation. The validation is done by calculating the left out measurement, $\hat{Y} = \Psi \cdot \hat{\Theta}$, with the model and then compare it to the real value.

Chapter 7

Measurements and Results

In this chapter two different measurements that were performed during this work are described. First, the proof-of-principle that shows that the instrument does in fact work with a mixture of different substances as theorized, is presented. Secondly, a measurement where the concentration of ethanol in water was measured.

7.1 Proof-of-principle

The instrument designed in this thesis was aimed to be able to measure concentrations of different substances that affect the optical properties in a sample. To prove that the instrument was able to do this a proof-of-principle (POP) measurement was performed. The measurement were done by starting with pure water and adding substances of known volume so that the concentration could be calculated. The substances were added in a glass cup standing on a magnetic stirrer for good mixing of the liquid. A peristaltic pump was used to pump the liquid through the quartz tube with a flow so that the liquid in the tube was refreshed once every second, i.e. the flow rate [cm^3/s] was equal to the volume [cm^3] of the quartz tube.

Five different substances were used that all changed the optical properties in different ways. Sugar mixed in water was used to change the refractive index, milk powder in a water solution introduced scattering in the system. Chlorophyll dissolved in acetone had a change in refractive index due to the acetone, a specific absorption spectrum and fluorescent effects. As pure absorbers green and red household colors were used mixed in water.

The more measurement values that are acquired the better the model and the fit will be. By taking ten measurements for every concentration the number of measurements was increased. This can be seen as the plateaus

in Fig. 7.3. Temporal behaviors such as incomplete mixing of the added substance and the sample can be seen as a change in concentration over the ten measurements of the same concentration. The calculated concentrations had to be compensated as more substances were added, e.g. if there is 10 ml of one substance in 100 ml liquid the concentration is 10% but if 20 ml of another substance is added the concentration of the first substance is only 8.3 %. This small decline in concentration over time can be seen in Fig. 7.3.

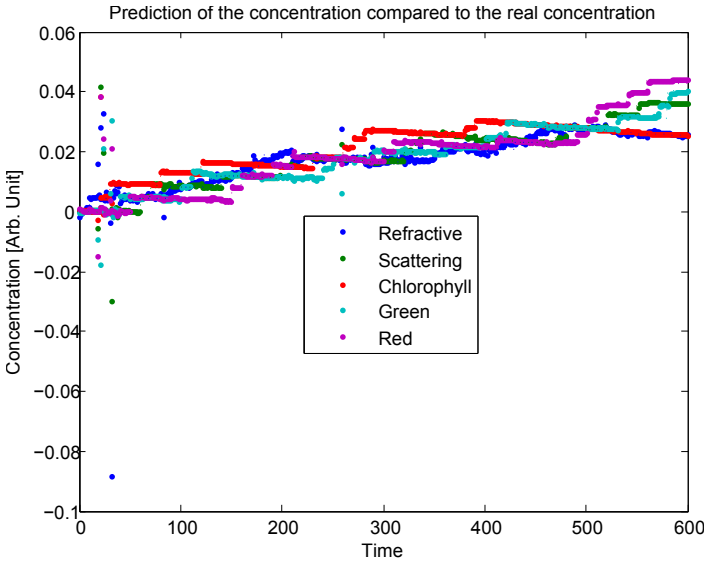

Figure 7.1: Predicted concentrations (dots) compared to the real concentrations (dotted lines) when no values have been removed which yields a bad model as can be seen by the negative concentrations predicted for the first measurements.

Figure 7.3 shows the predicted concentrations (dots) acquired from the leave-one-out method compared to the real concentrations (dotted lines) [1]. The first values where the concentration for all substances are low has been removed due to the fact that those values had a high uncertainty in the measurement and worsened the prediction of the rest of the measurements. The measurements where the concentration of one or more of the substances were zero was also needed to be removed when using the link function as the logarithm of zero is infinity.

[1]The concentration is given in an arbitrary value as the absolute concentration was unknown in the measurement. E.g. a few drops of green color was mixed with water, this solution was then used as the green "absorber". The concentration of the added substance was the same during the whole measurement but the absolute concentration unknown.

Substance	**Standard deviation** [%]	
	Quadratic model	Link function (ln)
Total	3.55	4.01
Refractive index	5.50	6.64
Scattering	2.39	1.76
Chlorophyll	1.52	1.46
Green color	3.73	3.09
Red color	3.33	4.67

Table 7.1: The standard deviations of the predicted values in the proof-of-principle with a quadratic model and a logarithmic link function truncated at 16 values.

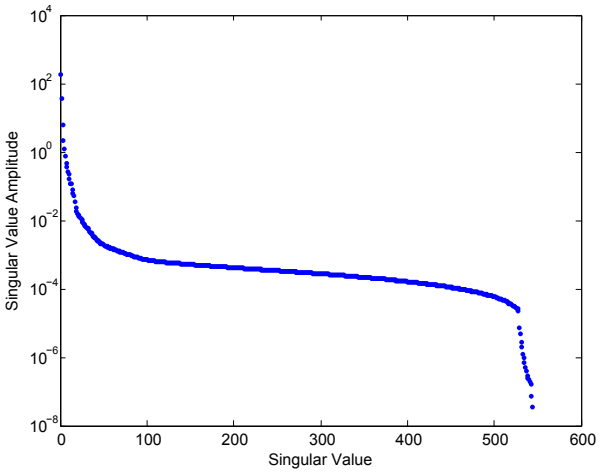

Figure 7.2: Singular values acquired from a decomposition made in the proof-of-principle measurements. The drop in amplitude of the singular values in the end could stem from duplicate measurements or outliers.

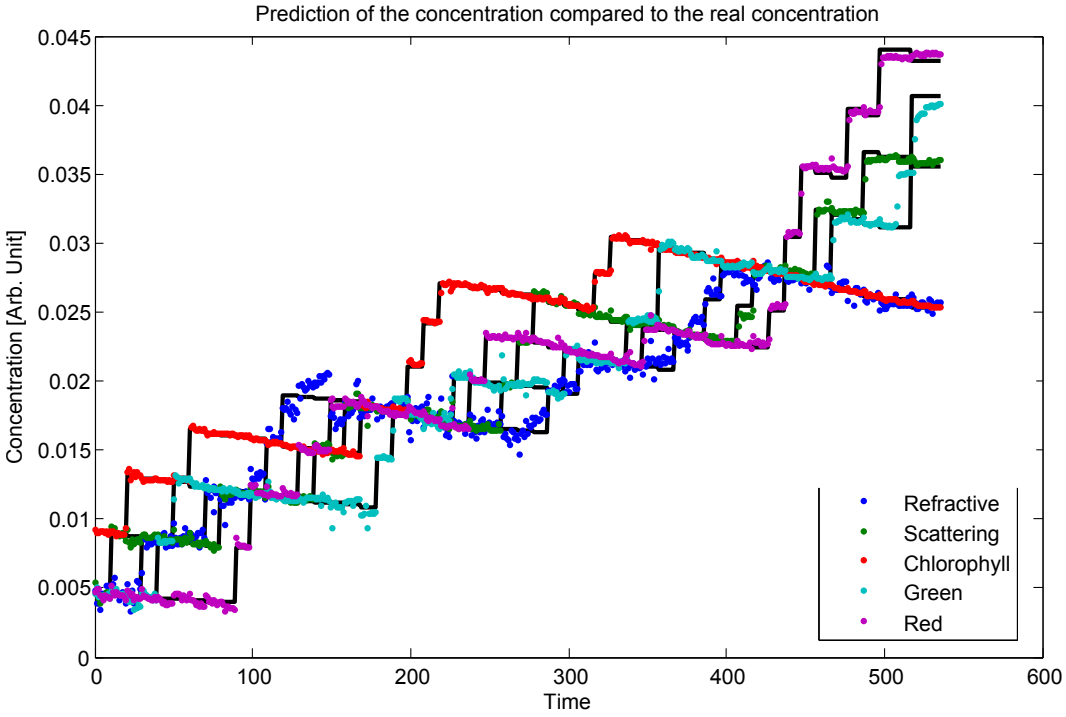

Figure 7.3: Predicted concentrations (dots) compared to the real concentrations (dotted lines).

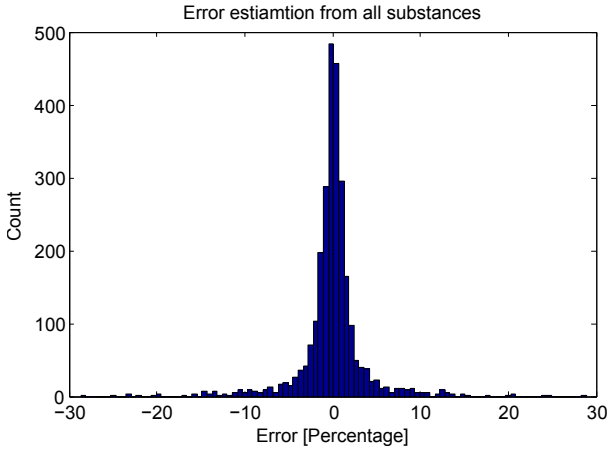

Percentual error of all substances.

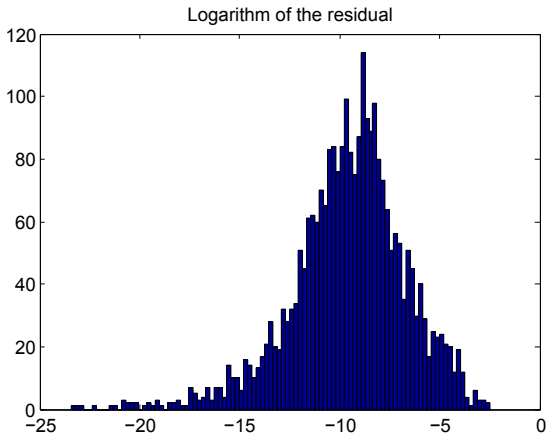

Logarithm of the squared residual.

Table 7.2: Two plots to visualize the error of the predictions for the proof-of-principle measurements.

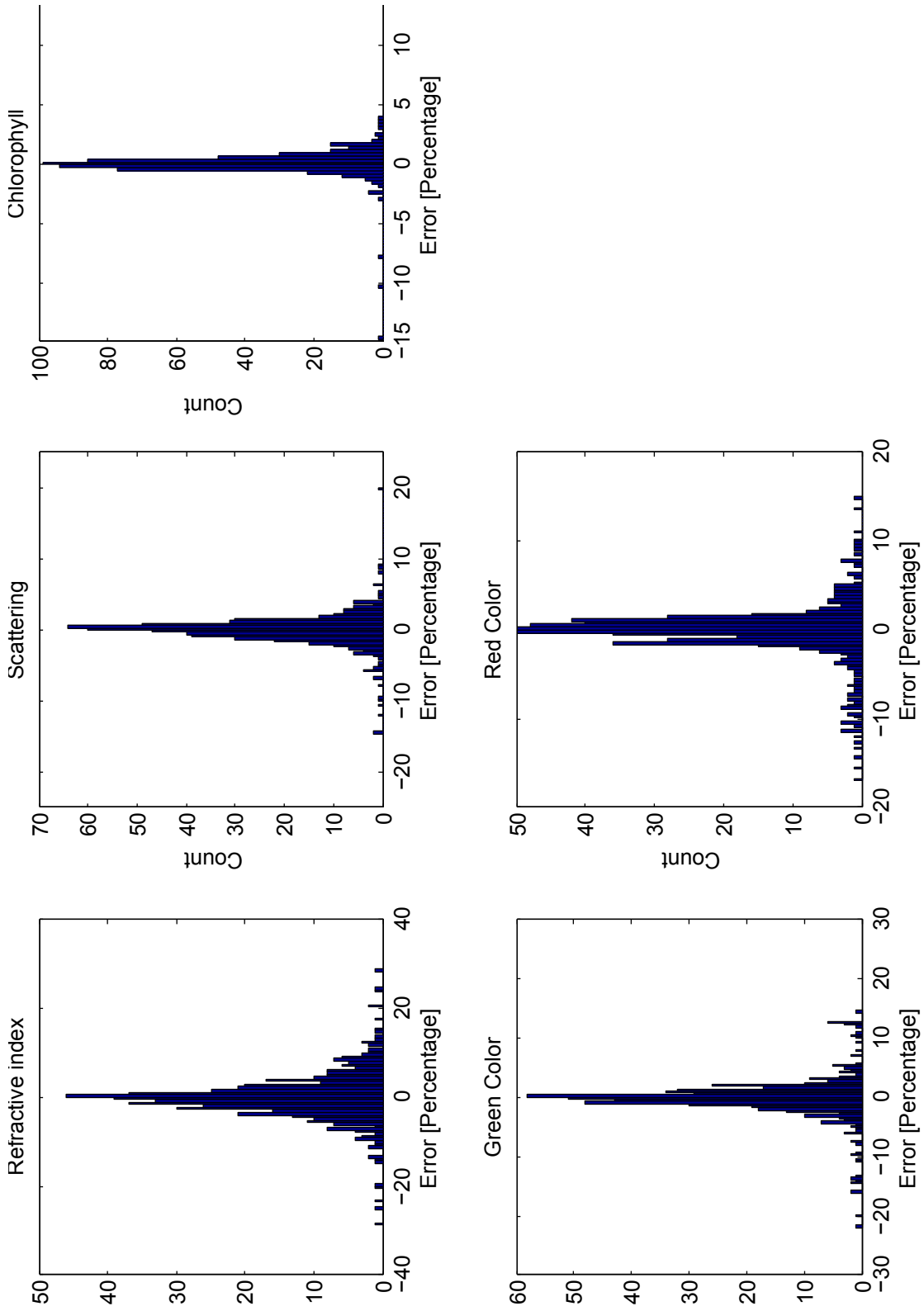

Figure 7.4: Error of each predicted value for every substance.

In the histogram of the error between the predicted and real concentrations, shown in Table 7.3 and Fig. 7.4, it can be seen that the error is normally distributed implying a random error and not a systematic one.

In Table 7.1 the standard deviations for the predicted values can be seen, both with a quadratic model and with a link function. It is seen that some standard deviations are better with the link function and some are worse.

7.2 Ethanol in water

In this section of the work, measurements on ethanol concentration were performed. Ethanol was mixed with water to acquire concentrations between 40% and 0%. Concentrations above 40% were tested but during these measurements the plastic tubing started to dissolve making the liquid solution foul and thereby changing the optical properties. No such phenomena were recorded for concentrations lower than 40%. Just as in the POP the measurements of the lower concentrations of ethanol (below 10%) has been removed to improve the prediction of the remaining measurements.

Model information	**Standard deviation** [%]
Quadratic model, 3 truncation values	1.90
Logarithmic link function, 3 truncation values	1.61

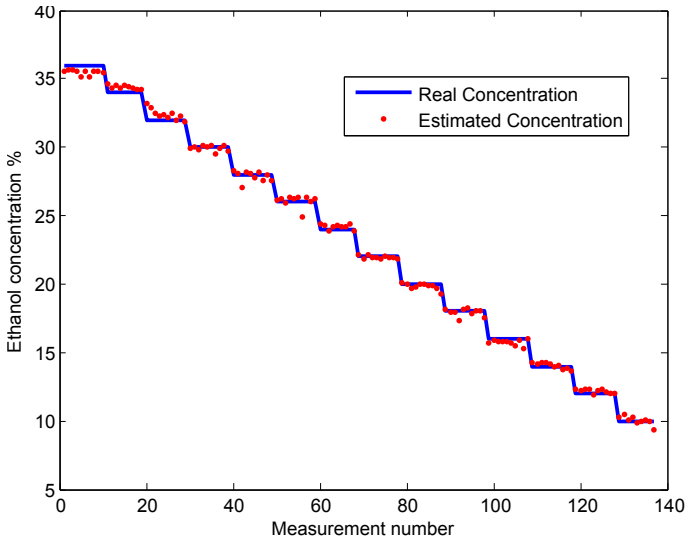

Figure 7.5: Predicted and real concentrations of ethanol in water.

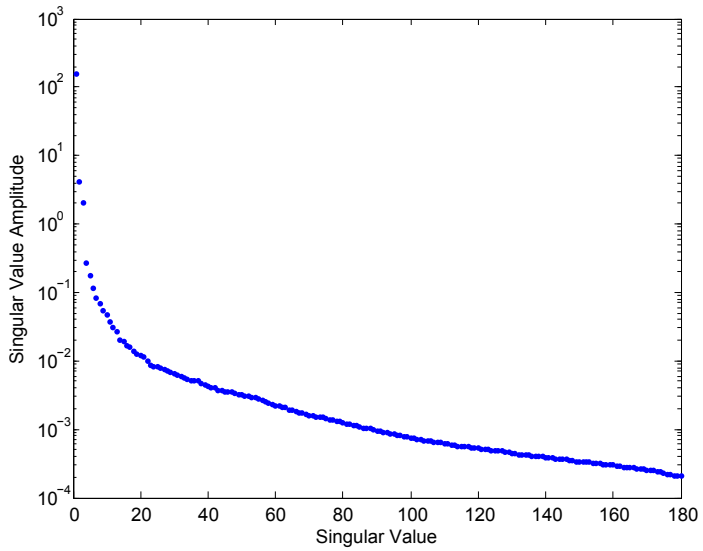

Figure 7.6: Singular value decomposition of ethanol measurements.

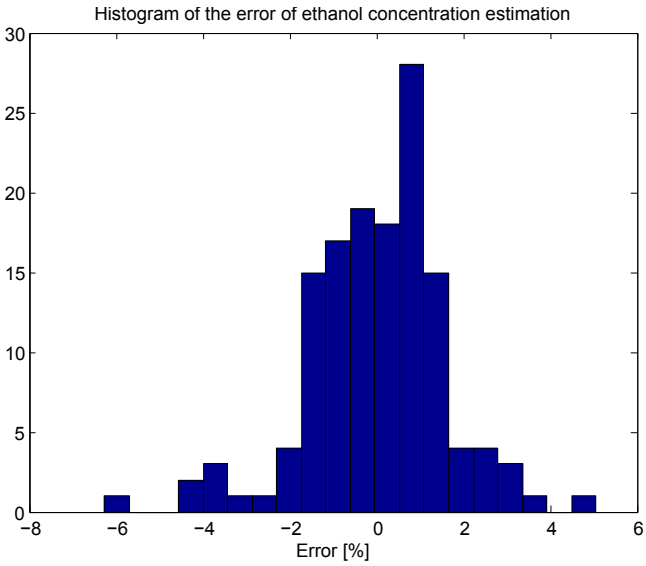

Percentual error of all substances.

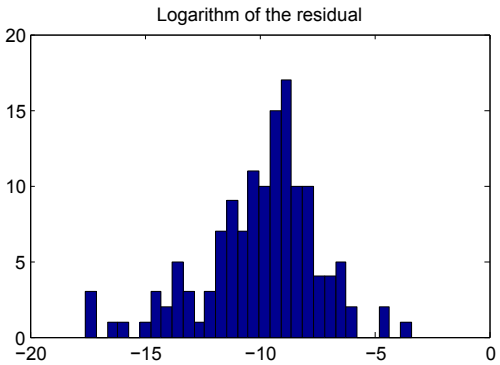

Logarithm of the squared residual.

Table 7.3: Two plots to visualize the error of the predictions for ethanol.

Chapter 8

Discussion

In this chapter the measurements and results will be analyzed and discussed. Comments will be given on the design of the instrument and how this has affected the measurements. Problems during the construction phase will be explained and the solutions for these problems given. It should be noted that a lot of practical work regarding electrical engineering has been put into this thesis.

The evidence presented in Chap 7 suggests that the method is viable for determination of unknown concentrations in a liquid. It is also seen that a turbid liquid does not interfere with the ability of the instrument to determine the optical properties of a liquid sample. A total standard deviation of 3.55% for the proof-of-principle has to be seen as an acceptable value at this stage of the instrument development. Possible improvements will be suggested in the next chapter. The difference between two measurements done on an identical sample were observed to be a few per mille.

8.1 Electrical engineering

During the construction of the instrument some electrical related problems did occur as is to be expected of work of this kind. One of the bigger issues was the failure of some transistors that were of the field effect kind (FET). These were replaced with another type of transistor, the bipolar junction transistor (BJT), which are not as likely to break. For future projects it can be recommended to use BJT when considering what kind of transistor that should be used to save time trouble shooting a circuit board.

Another electrical related problem occurred during the data acquisition process. In the digitalization of the analogue voltages from the photodiodes some ghosting was observed for channels recorded just after the common

anode. Ghosting means that a measurement is affected by the signal that was registered in the channel before. It was theorized that this issue could arise from the fact that the DAQ card only has one A/D-converter resulting in that when multiple channels are measured a multiplexer has to switch between the different channels and a capacitance can give rise to the ghosting. The ghosting was solved by decreasing the number of channels measured at the same time, and by putting an empty channel after the common anode.

8.2 Proof-of-principle

The proof-of-principle measurements were a success with respect to that the instrument proved to be able to measure the concentrations. The absolute best predictions of a concentration in the proof-of-principle work were made for the chlorophyll., with a standard deviation of only 1.52% for the quadratic model used. One reason for the good predictions is that the chlorophyll affects three different optical properties, a refractive index change due to being solved in acetone, fluorescent effects and absorption of some wavelength covered by the instrument.

Examining Fig. 7.3 more closely, it can be seen that the substance that has the worst predictions is the sugar-water mix, which only changes the refractive index. The predictions follow the pattern of the real concentrations to a certain degree. This observation is further reinforced when investigating the histograms of the errors as it can be seen that the histogram for the refractive index prediction is the broadest. The standard deviation is the largest for the refractive index measurements. A possible explanation could be that the change in refractive index is not large enough, which makes the measurements uncertain.

In the data analysis a lot of time can be invested in developing the best model possible. This involves determining the amount of truncation values; what kind of model that is used; if any link functions should be used and possibly removing outliers which to some extent will always be present as there is always one measurement that is the worst. The issue with this is that the model is only viable for precisely this measurement series. When a new measurement is done a new method has to be developed. In this work the truncation number and model were chosen after some testing and the best results are presented in this report.

As it is now absolute measurements are used in the data analysis which means that no consideration is taken if there is a difference in LED intensity. Relative measurements (unitless) can be introduced by dividing a measurement with another measurement, e.g. for pure water. This was done for the

proof-of-principle tests but yielded bad results. The results were heavily influenced by small disturbances. When a measurement sequence is acquired, voltages from some photodiodes will be very low, e.g. if the LED and photodiode are far from each other. A small disturbance such as temporary noise will affect the division a lot as two values very close to zero are divided.

As mentioned in Chap. 7, the measurements for the lowest concentrations had to be removed to improve the predictions from the model. A reason for this could be that the model is a bad fit for lower concentrations mentioned in Sec. 6.3.2. A logarithmic link function can not be used to improve the model since some of the concentrations are zero for these first measurements.

8.3 Ethanol

The ethanol measurements shown in Sec. 7.2 reveal that it is possible to measure the absolute ethanol concentration in water. Ethanol differs from water in both the refractive index and the absorption spectrum. Transmittance for ethanol in the near-IR is shown in Fig. 8.1 and for water in Fig. 8.2.

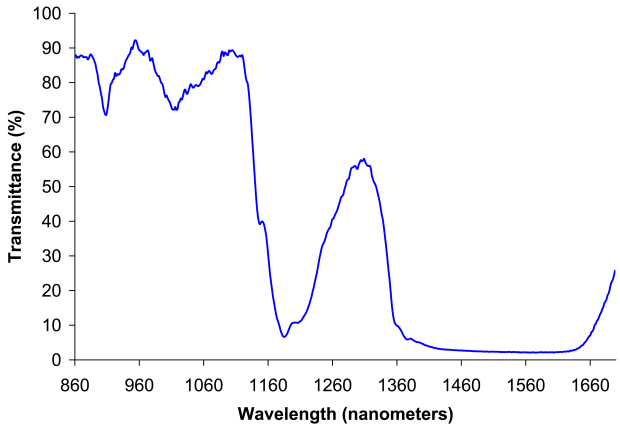

Figure 8.1: Near-IR absorption spectrum of ethanol.

The standard deviation when determining the concentration of ethanol between 40% and 10% was 1.61% which is very acceptable. For lower concentrations the same issue as in the proof-of-principle measurements arises with bad predictions. Even with a logarithmic model no improvement was made.

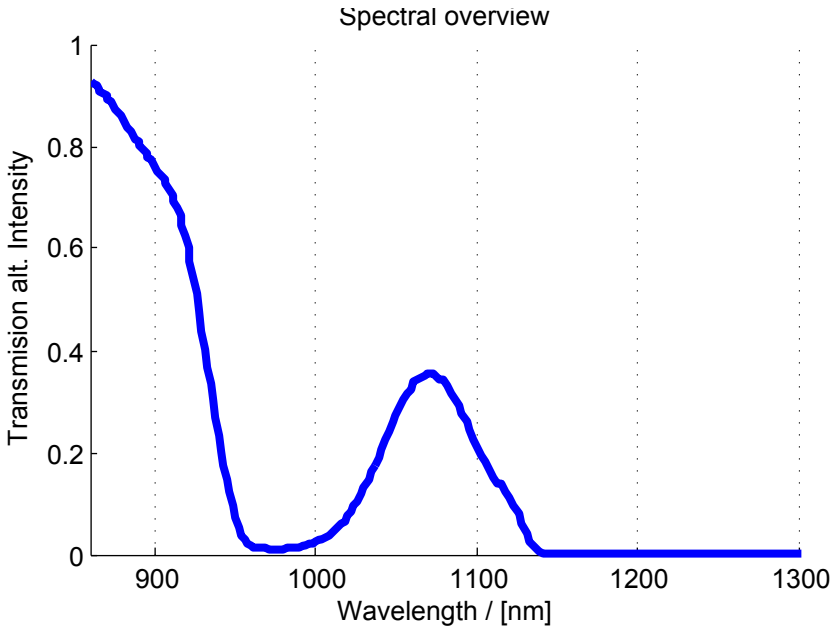

Figure 8.2: Near-IR absorption spectrum of water.

Comparing the singular value plots from the proof-of-principle measurements and from the ethanol measurements it can be seen that there are less significant values in the ethanol measurement. This is to be expected according to theory as there are less optical properties that vary.

The instrument can also be used as a spectrometer with 15 spectral bands, i.e. the number of different light sources used. This can be visualized by plotting the measured intensity from a photodiode opposite to a LED. A spectral plot comparing water and green color can be seen in Fig. 8.3, where the spectra have been normalized to pure water. Here it is seen that wavelengths not lying in the green range is attenuated.

A broadening effect when scattering is added to a liquid can be seen in Fig. 8.4.

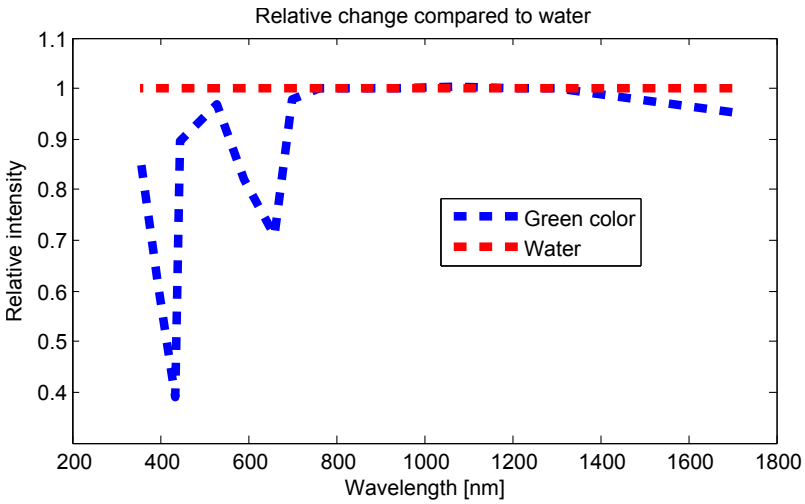

Figure 8.3: The instrument used as a spectrometer. Comparing water (red dots) with green color (blue dots). Both curves are normalized with a pure water spectrum.

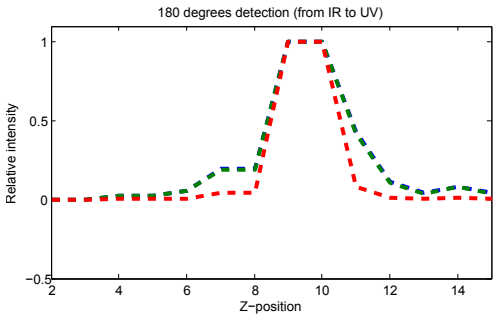

Figure 8.4: A broadening effect can be seen when scattering is added.

Chapter 9

Outlook

In the work performed during this thesis it has been shown that an instrument (Combinatorial Light Path Spectrometer, CLPS) constructed from relatively low-cost electronic components can measure concentrations of substances in a liquid as long as the optical properties change. The CLPS is a very promising technique that may have great usage in the industry because of its ability to measure on different substances at a low cost and without any interfering cross-talk. The major expense in the design of this instrument was the DAQ card costing about 1500 €. A rough estimate of the total cost would land on 2500 €, which has to be considered cheap, accounting for the endless possibilities of measurements that the instrument allows for.

A practical issue that arises from the current construction is that the quartz tube will aggregate a dirty coating on the inside when the liquid is pumped through the tube. Depending on the liquid this will happen at different rates. The coating will decrease the transmission of light and decrease the quality of the measurement due to that the interesting information will constitute small fluctuations on a large background. As the instrument is designed at the moment, the quartz tube is easily interchangeable but if the system is mounted in an industry this may not be the case. A solution could be that the tube is removed and the copper bar mounted vertically letting the liquid flow laminarly through the illumination/detection zone.

There are numerous modifications and changes that can be made to the design of the tube. By modulating the light at radio frequencies the phase delay of the light, the time it takes for the light to get from the source to the detector, will be possible to measure. Allowing the time of flight to be calculated, for fluorescence the photon delay can be expected to be longer. Doing measurements for different radio frequencies will give the possibility to calculate the phase shift. Polarization measurements can be done by adding more light sources.

Acknowledgements

I would like to thank everyone in the *Applied molecular spectroscopy and remote sensing* group at the Atomic Physics Division, LTH, for the discussions we have had that has helped me a lot. Special thanks to Hiran Jayaweera for the great help and input I received throughout the whole time of this work.

My supervisors Sune Svanberg and Mikkel Brydegaard deserves a big recognition for allowing me to conduct this work and for the support and time they have put into helping me.

Bibliography

[1] U. Platt and J. Stutz. *Differential Optical Absorption Spectroscopy: Principles and Applications*. Springer, 2008.

[2] A. Bohlin, F. Vestin, P. Joubert, J. Bonamy, and PE. Bengtsson. Improvement of rotational CARS thermometry in fuel-rich hydrocarbon flames by inclusion of $N_2 - H_2$ raman line widths. *Journal of Raman spectroscopy*, 40(7):788–794, 2009.

[3] S. Svanberg. *Multi-Spectral Imaging: from Astronomy to Microscopy*. Department of Physics (compendium), 2008.

[4] T. L. Bergman, F. P. Incropera, and W. H. Stevenson. Miniature fiber-optic refractometer for measurement of salinity in double-diffusive thermohaline systems. *Review of Scientific Instruments*, 56(2):291 –296, 1985.

[5] Y. Zhao, Z. Bo, and L. Yanbiao. Experimental research and analysis of salinity measurement based on optical techniques. *Sensors and Actuators B: Chemical*, 92(3):331 – 336, 2003.

[6] S. Shyam. Refractive index measurements and its applications. *Physica Scripta*, 65(2):167 – 180, 2002.

[7] S. Svanberg. *Atomic and Molecular Spectroscopy: Basic Aspects and Practical Applications*. Springer, 2004.

[8] http://refractiveindex.info/, Recorded 2010-01-06.

[9] K. Fuwa and B. L. Valle. The physical basis of analytical atomic absorption spectrometry. the pertinence of the beer-lambert law. *Analytical Chemistry*, 35(8):942 – 946, 1963.

[10] L. Persson. *Laser Spectroscopy in Scattering Media for Biological and Medical Application*. PhD Dissertation, LTH, 2007.

[11] M.H. Chiu, J.Y. Lee, and D.C. Su. Complex refractive-index measurement based on fresnel's equations and the uses of heterodyne interferometry. *Appl. Opt.*, 38(19):4047–4052, 1999.

[12] B. Drevillon, J. Perrin, R. Marbot, A. Violet, and J. L. Dalby. Fast polarization modulated ellipsometer using a microprocessor system for digital fourier analysis. *Review of Scientific Instruments*, 53(7):969 – 977, 1982.

[13] M. Bader. A systematic approach to standard addition methods in instrumental analysis. *Journal of Chemical Education*, 57(10):703, 1980.

[14] E.W. C. Gributs and H. D. Bruns. Multiresolution analysis for quantification of optical properties in scattering media using pulsed photon time-of-flight measurements. *Analytica Chimica*, 490(1-2):185 – 195, 2003.

[15] T. Svensson, E. Alerstam, D. Khoptyar, J. Johansson, S. Folestad, and S. Andersson-Engels. Near-infrared photon time-of-flight spectroscopy of turbid materials up to 1400 nm. *Review of Scientific Instruments*, 80(6):063105, 2009.

[16] Jiang F., Lee F., Wang X., and Dai D. The application of excitation/emission matrix spectroscopy combined with multivariate analysis for the characterization and source identification of dissolved organic matter in seawater of bohai sea, china. *Marine Chemistry*, 110(1-2):109 – 119, 2008.

[17] A. Baker. Fluorescence excitation-emission matrix characterization of some sewage-impacted rivers. *Environmental Science and Technology*, 35(5):948–953, 2001.

[18] A. M. K. Nilsson, C. Sturesson, D. L. Liu, and Andersson-Engels S. Changes in spectral shape of tissue optical properties in conjunction with laser-induced thermotherapy. *Appl. Opt.*, 37(7):1256 – 1267, 1998.

[19] A.M.K. Nilsson, G.W. Lucassen, W. Verkruijsse, S. Andersson-Engels, and M.J.C. van Gemert. Changes in optical properties of human whole blood in vitro due to slow heating. *Photochemistry and Photobiology*, 65(2):366 – 377, 1997.

[20] M.S. Thompson, Johansson A., Johansson T., S. Andersson-Engels, S.and Svanberg, N. Bendsoe, and K. Svanberg. Clinical system for in-

terstitial photodynamic therapy with combined on-line dosimetry measurements. *Appl. Opt.*, 44(19):4023 – 4031, 2005.

[21] Zhu T. C., Dimofte A., Finlay J. C.and Stripp D., Busch T., Miles J., Whittington R., Malkowicz S. B., Tochner Z., Glatstein E., and Stephen M. Hahn. Optical properties of human prostate at 732 nm measured in vivo during motexafin lutetium mediated photodynamic therapy. *Photochemistry and Photobiology*, 81:96 – 105, 2005.

[22] J. Swartling, J. Axelsson, G. Ahlgren, K.M. Kalkner, S. Nilsson, S. Svanberg, K. Svanberg, and S. Andersson-Engels. System for interstitial photodynamic therapy with online dosimetry: first clinical experiences of prostate cancer. *Journal of Biomedical Optics*, 15:058003, 2010.

[23] I. T. Jolliffe. *Principal Component Analysis*. Springer, 2002.

[24] E. F. Schubert. *Light Emitting Diodes, Second Edition*. Cambridge Univeristy Press, 2006.